60 GHz Aperture-Coupled Dielectric Resonator Antennas Fed by a Half-Mode Substrate Integrated Waveguide

Qinghua Lai, *Graduate Student Member, IEEE*, Christophe Fumeaux, *Senior Member, IEEE*, Wei Hong, *Senior Member, IEEE*, and Rüdiger Vahldieck, *Fellow, IEEE*

***Abstract*—Dielectric resonator antennas (DRAs) fed by a half-mode substrate integrated waveguide (HMSIW) are proposed and studied in this paper. The investigated antenna configuration consists of a dielectric resonator (DR) mounted on the conducting back plane of an HMSIW. Energy is coupled from the interior HMSIW to the DR through an aperture between them. Using this excitation scheme, a 60 GHz linearly polarized HMSIW-fed DRA is first designed by applying a transverse rectangular slot to feed a dielectric cylinder. This design experimentally exhibits a bandwidth of 24.2% for $S_{11} < -10$ dB. In particular, a gain higher than 5.5 dB and a radiation efficiency between 80% and 92% are obtained over the whole operation band, indicating that the HMSIW can be an efficient feed for DRAs operating around 60 GHz. In addition to this linearly polarized example, a DRA of circular polarization, coupled through a pair of cross slots, is also designed, presenting a measured 3-dB axial ratio bandwidth of 4.0%.**

***Index Terms*—Dielectric resonator antennas (DRAs), half-mode substrate integrated waveguide (HMSIW).**

I. Introduction

SINCE the first application of a cylindrical dielectric resonator as an antenna [1], a number of excitation schemes have been proposed for the dielectric resonator antennas (DRAs) [2]–[6]. One of the most common feeding mechanisms consists in coupling energy into the resonator through an aperture in its ground plane. This technique can be applied in conjunction with various transmission lines, including the conventional rectangular waveguide [7] and various planar waveguides such as the microstrip line [8], [9], coplanar waveguide [10], and substrate integrated waveguide [11]. One distinguished advantage of the aperture-fed DRAs is the easy realization of the desired polarization, which can directly be implemented either by selecting suitable slot shapes [8], [9], [12]–[14] or by adjusting the relative position between the slot and resonator [15]. In some cases, a wide operation bandwidth can also be conveniently achieved by merging offset resonances of the slot and dielectric resonator [16], i.e., these two resonances are placed on each side of the center frequency of interest and their combined frequency ranges determine the bandwidth of operation. Furthermore, aperture-coupled DRAs based on planar waveguides appear as a competitive antenna choice for antenna-in-package designs at mm-wave frequencies, considering their compatibility with integrated circuits and their high radiation efficiency [17]. However, some drawbacks associated with the feeding transmission line need to be taken into account when considering a DRA for a given application. For example, for the DRAs fed by a microstrip line, the overall radiation efficiency might drastically degrade with rising frequency, due to the increasing conductor and radiation losses in the feeding microstrip line. Another illustrative example is the DRAs fed by a substrate integrated waveguide (SIW), for which the large transverse size of the feeding SIW might become a barrier for some application. Despite the restrictions imposed by the SIW transverse size, it is worth noting that the SIW can be an attractive alternative to the microstrip line as a feed for DRAs operating in the millimeter wave band, when considering the high quality factor of the SIW.

In an effort to create a compact and efficient feeding scheme for DRAs operating at millimeter wave frequencies, a novel excitation structure based on a half-mode substrate integrated waveguide (HMSIW) is proposed and studied throughout this work. The concept of HMSIW was first proposed in [18] and since then, a number of high-performance devices have been developed with this technique, including filters [19], [20] antennas [21], and power dividers [22]. Recently, a theoretical and experimental study has been carried out to characterize the propagation properties of the HMSIW [23]. The investigation results have demonstrated that for an HMSIW and a standard 50-Ω microstrip line fabricated on the same substrate, the HMSIW can present an attenuation constant much smaller than the microstrip line at frequencies above 40 GHz. This motivates the introduction of the HMSIW as feed for the DRAs. Sketches of the investigated antenna configuration are shown in Fig. 1. A cylindrical dielectric resonator is mounted on the conducting back plane of an HMSIW and the energy is coupled from the interior waveguide to the dielectric resonator through an aperture that is etched into the HMSIW back plane, beneath the dielectric cylinder. Fig. 1(b) shows that the HMSIW is fed by a

Manuscript received May 25, 2009; revised November 04, 2009; accepted December 16, 2009. Date of publication March 29, 2010; date of current version June 03, 2010. This work was supported in part by the Laboratory for Electromagnetic Fields and Microwave Electronics at ETH Zurich and in part by the NSFC under grant 60621002 from China.

Q. Lai and W. Hong are with the State Key Lab. of Millimeter Waves, School of Information Science and Engineering, Southeast University, Nanjing 210096, China (e-mail: qhlai@emfield.org).

C. Fumeaux is with the School of Electrical and Electronic Engineering, The University of Adelaide, Adelaide 5005, South Australia (e-mail: cfumeaux@eleceng.adelaide.edu.au).

R. Vahldieck is with the Laboratory for Electromagnetic Fields and Microwave Electronics, ETH Zürich, Zürich CH-8092, Switzerland (e-mail: vahldieck@ifh.ee.ethz.ch).

Digital Object Identifier 10.1109/TAP.2010.2046852

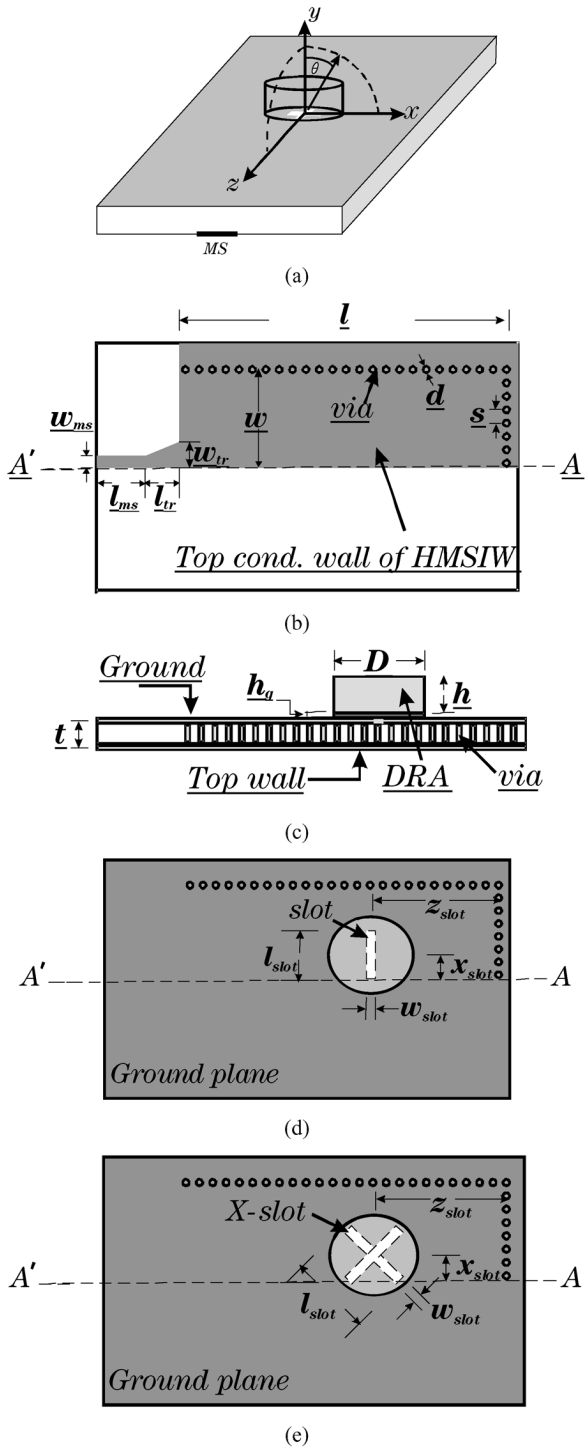

Fig. 1. Sketches of the HMSIW-fed DRAs. (a) 3D view. (b) View of the HMSIW feeding side. The substrate is shown as white and the dark gray areas are metalized. The metal posts (vias) are shown as circles. The width and length are w and l for the HMSIW, $w_{\rm ms}$ and $l_{\rm ms}$ for the microstrip line, and $w_{\rm tr}$ and $l_{\rm tr}$ for the taper impedance transition. The vias diameter is d and the spacing between them is s. (c) Side view. The dielectric cylinder has a diameter D and a height h. The glue layer thickness is $h_{\rm g}$ and the substrate thickness is t. (d) Top view of a linearly polarized HMSIW-fed DRA. The cylindrical dielectric resonator is shown as circular area in light gray and the slot is plotted as a rectangle in white. The slot has a width $w_{\rm slot}$ and a length $l_{\rm slot}$. The slot center has a distance of $z_{\rm slot}$ from the HMSIW shorted end and a distance of $x_{\rm slot}$ from the HMSIW open side. (e) Top view of a circularly polarized HMSIW-fed DRA.

microstrip line through a tapered impedance transition at one end, and is shorted by a column of metallic vias at the other end. As depicted in Fig. 1(d), a transverse rectangular slot is applied to feed the dielectric cylinder for linearly polarized radiation, while a pair of cross slots is adopted for realizing circular polarization as illustrated in Fig. 1(e). Design procedures are first described for both types of antennas in Section II. Subsequently, the measured performance of two fabricated prototypes, of linear and circular polarization respectively, is demonstrated for 60 GHz operation in Section III. The good agreement between the measured and simulated results validates the concept of the HMSIW-fed DRA as a high efficiency feed-antenna combination for millimeter-wave band applications.

II. Design Procedures

In this section, design approaches are sequentially described firstly for the linearly polarized and secondly for circularly polarized HMSIW-fed aperture-coupled DRAs.

A. HMSIW-Fed DRAs of Linear Polarization

HMSIW Dimensions: The first step in the design procedure is to determine the dimensions of the feeding HMSIW. For a practical antenna design, the HMSIW cutoff frequency f_c is first appropriately selected by considering that the whole operation frequency band of the DRA should be on one hand far away from the HMSIW cutoff frequency, and on the other hand, still within the single mode operation region of the waveguide. A full design methodology for the HMSIW has been presented in [23] and is only briefly outlined here. Based on the cutoff frequency f_c, an HMSIW effective width w_{eff} can be calculated using [23, Eq. (11)]. Subsequently, the substrate thickness t and permittivity ε_r as well as the metallic vias diameters d and spacing s are properly selected to guarantee a good confinement of fields inside the HMSIW [24]. Lastly, substituting the known parameters w_{eff}, t, ε_r, d, and s into [23, Eq. (8)–(10), (13)] yields the HMSIW physical width w, which is the only unknown in that set of design formulas.

Dielectric Resonator Dimensions: Explicit formulas are available in the literature for determining the resonant frequencies of dielectric resonators according to their shapes, dimensions, and operation modes [25]. In general, a non-unique set of dimensions can make dielectric resonators of a given shape operate at a specified resonant frequency on the same mode. Therefore, care should be taken to select an appropriate set of dimensions by considering the antenna specifications and fabrication aspects. For instance, the dielectric cylinder used in our work is designed to operate on the $HEM_{11\delta}$ mode and its dimensions, i.e., its height h and diameter D, are calculated from [25, Eq. (5)]. A large diameter-to-height ratio is chosen for the cylindrical resonator out of consideration to obtain a broad bandwidth [26], while lowering the antenna profile and providing large space to flexibly tune the coupling slot length.

Slot Location and Dimensions: As only a small amount of energy leaks from the waveguide into the uncovered substrate area (the region in white in Fig. 1(b)), the whole slot is cut inwards the HMSIW as shown in Fig. 1(d). Furthermore, in order to maximize energy coupling from the HMSIW interior to the dielectric resonator, the slot is positioned at a distance of $z_{slot} = n\lambda_g/2\ (n = 1, 2, \cdots)$ from the HMSIW shorting end.

The guided wavelength λ_g can be calculated according to the relation $\lambda_g = 2\pi/k_z$, where the phase constant k_z can be determined by [23, Eq. (12)].

The slot width is selected as $w_{slot} < \lambda_0/20$ in order to avoid cross-polarized radiation, where λ_0 is the resonant wavelength in free space. The slot length $l_{\rm slot}$ is optimized with the aid of the electromagnetic simulation tool Ansoft HFSS. This optimization process on one hand helps achieve the impedance matching between the HMSIW and dielectric resonator, and on the other hand, enables combining the offset resonances of the slot and dielectric resonator [16] to produce a broadband antenna.

Impedance Matching Network: For the sake of measurements, a microstrip line is used to feed the HMSIW. The impedance matching between the feeding microstrip line and the HMSIW can be realized through an intermediate microstrip taper, as shown in Fig. 1 with optimized dimensions w_{tr} and l_{tr}.

B. HMSIW-Fed DRAs of Circular Polarization

For the case of circularly polarized HMSIW-fed DRAs, the design of the HMSIW, dielectric resonator, and matching network can be carried out using the same methods as for the linearly polarized HMSIW-fed DRAs. Therefore, the following design procedure concentrates firstly on the positioning of the coupling slots and secondly on the determination of their dimensions.

Positioning of the X-Slot: It is known that a pair of crossed slots cut into the broad wall of a rectangular waveguide can radiate circularly polarized wave, if the X-slot is located at the points where the transverse and longitudinal magnetic field components of the dominant TE_{10} mode are equal in amplitude [27]. Considering that the dominant $TE_{0.5,0}$ mode in an HMSIW of width w is approximately half the dominant TE_{10} mode in a rectangular waveguide of width $2w$ [22], [23], the X-slot used in the circularly polarized HMSIW-fed DRAs should also be centered at the spots where two orthogonal magnetic field components of the dominant $TE_{0.5,0}$ mode have an identical amplitude.

Fig. 2 depicts an X-slot etched on the conducting back wall of an end-shorted HMSIW which extends to infinity along the $+z$ direction. Field equations have been derived as [23, Eq. (4)] for the dominant traveling wave in a thru-HMSIW. By reformulating those equations and adapting them to the coordinates of Fig. 2, two expressions can be obtained for the two magnetic field components of the standing $TE_{0.5,0}$ mode in the shorted HMSIW as follows:

$$H_x = \frac{-A}{\omega\mu} k_x k_z \sin k_x(w-x)\cos k_z z \tag{1a}$$

$$H_z = \frac{-A}{\omega\mu} k_x^2 \cos k_x(w-x)\sin k_z z \tag{1b}$$

in which ω is the angular frequency, μ is the permeability of substrate, w is the HMSIW width, and A is a real amplitude constant. Wave numbers k_x and k_z are in the form of [23, (3)].

A comparison of (1a) and (1b) indicates that the two magnetic components H_x and H_z have an inherent 90° phase difference. Therefore, circular polarization will be radiated at the spots where the two components are equal in amplitude. With the relation of $|H_x| = |H_z|$, the following equation can be derived to determine possible locations of the X-slot center

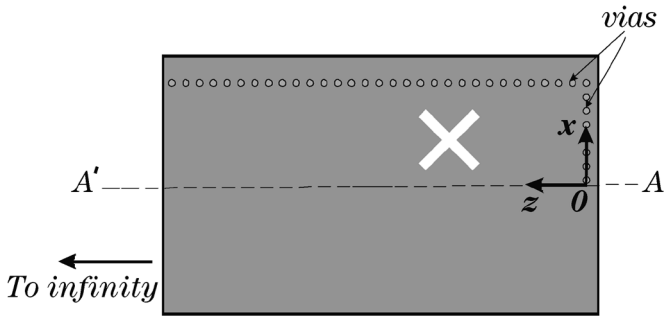

Fig. 2. An X-slot etched on the conducting back plane of an end-shorted HMSIW. It is noted that the origin of current coordinate system is located at the corner of the HMSIW, compared to that in Fig. 1 placed at the cylinder center.

$$x = w - \frac{1}{k_x}\operatorname{arc\,cot}\left(\pm\frac{k_z}{k_x}\cot k_z z\right). \tag{2}$$

It is noted that for a given certain value of z, two values of x can be obtained by adopting "+" or "−" in (2), respectively. But only the value of $x \in (0, w)$ is physically valid as the X-slot is centered within the HMSIW.

For illustration purpose, Fig. 3 plots a curve computed with (2), corresponding to the example of circularly polarized HMSIW-fed DRA described in the present work. The antenna is designed for ideal circular polarization at broadside at 60 GHz. The feeding HMSIW has a width $w = 2.35$ mm, a height $t = 0.127$ mm, and substrate permittivity $\varepsilon_r = 2.2$. The maximum electric field in the HMSIW across section is estimated to occur at the spot of $x = 0.1w$ according to [23, Fig. 4]. That is to say the value of the parameter a in [23, Eq. (3)] is assessed at $0.1w$. A mapping of Fig. 3 onto Fig. 2 shows that boundaries of Fig. 3 at $z = 0$, $x = 0$, and $x = 2.35$ mm correspond to the shorted end, open side, and shorted side of the HMSIW, respectively. The curve is divided into segments, where the solid lines are related to the use of '+' in (2), indicating $H_x = H_z$, while the dash lines result from the adoption of "−" in (2), representing a relation of $H_x = -H_z$. Depending on the excitation type, i.e., $H_x = H_z$ or $H_x = -H_z$, either circular polarization sense (i.e., clockwise or counterclockwise) can be excited by centering the X-slot on either branch of the line. It is noted that the possible positions for the two circular polarization senses alternate with a period of half a guided wavelength along z-axis, coinciding with the cyclic behavior of (2).

To validate (2), a model of slotted HMSIW in the configuration of Fig. 2 is analyzed using HFSS. The HMSIW and the pair of slots are identical with their counterparts in the circularly polarized HMSIW-fed DRA, whose dimensions are given in Table I. Varying the X-slot position on the conducting back wall of the HMSIW, a minimum value of axial ratio can be observed at 60 GHz at some spots where the two magnetic components are considered in the equal amplitude, i.e., $|H_x| = |H_z|$. The coordinates of the optimal locations are recorded and then marked in star symbols in Fig. 3. A fairly good agreement is gained between the calculation and simulation results, validating the

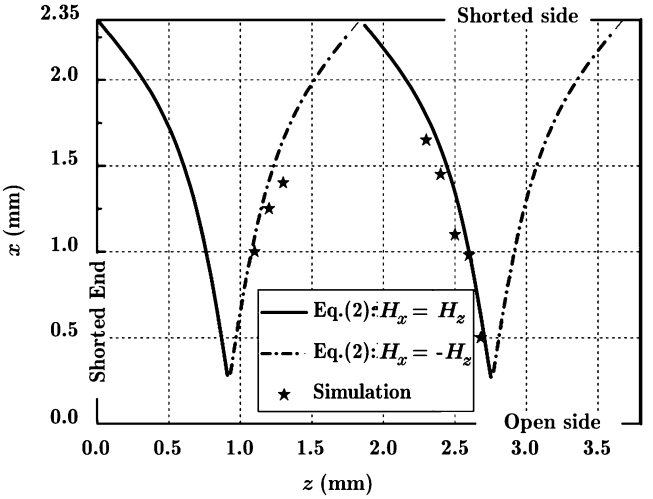

Fig. 3. Position of the X-slot center on the conducting back wall of the HMSIW for radiating circularly polarized wave.

proposed design (2). It is noted that due to the HMSIW small thickness, the etching of the X-slot distorts the field distribution inside the waveguide. That effect is not considered in the derivation of (2), which mainly explains the discrepancy between the calculations and simulations.

Finally, it is pointed out that although an infinite number of points can be theoretically calculated from (2), only those close to the middle of the HMSIW ($x \approx w/2$) can be used in practice, as the slot has to be entirely etched within the HMSIW.

Slot Dimensions: As in the case of linearly polarized antenna, the pair of slots has a width much smaller compared to the wavelength in free space ($< \lambda_0/20$). In order to excite two near-degenerate orthogonal modes in the dielectric cylinder, two slots are orthogonally crossed and have identical or slightly different lengths [12], [14].

Theoretically, for a pair of identical cross slots, the center positioning obtained from (2) can guarantee a circularly polarized radiation regardless of the slot length [27], which significantly simplifies the design. However, in order to obtain sufficient coupling from the HMSIW interior to the dielectric resonator, an optimal slot length is empirically found around $\lambda_g/2$, where λ_g is the guided wavelength calculated from the relation $\lambda_g = 2\pi/k_z$, as in the previous case of linearly polarized antennas. In the real design, due to the distortion effects of the X-slot on the field distribution beneath the aperture inside the HMSIW, the individual slot length might have to be optimized slightly for achieving a desired axial ratio level as well as for merging the impedance band (where $\mathrm{S}_{11} < -10$ dB) and the axial ratio band (where $\mathrm{AR} < 3$ dB). Therefore, the resulting optimized slots might have slightly different lengths. It is worth emphasizing that, since the polarization sense is only dependent on the slot location, i.e., either on the solid branch or dash branch, exchanging the slot lengths does not change the circular polarization sense for the present HMSIW-fed circularly polarized DRA.

Up to this point, design approaches have been given for the proposed HMSIW-fed aperture-coupled DRAs of linear and circular polarizations.

TABLE I
CONFIGURATIONS OF TWO TYPES OF HMSIW-FED DRAS

UNIT: MM

Parameter	LP	CP	Parameter	LP	CP
w_{ms}	0.35	0.35	D	3.0	2.0
l_{ms}	10.0	10.0	h	0.5	0.7
w_{tr}	0.90	0.30	x_{slot}	1.0	1.0 ± 0.02
l_{tr}	1.40	2.40	z_{slot}	2.30	2.75
w	2.20	2.35	w_{slot}	0.20	0.20
l	8.90	8.55	l_{slot}	2.0	2.0
d	0.40	0.40	h_{g} (um)	15 ± 5	15 ± 5
s	0.50	0.50	t (mil)	5	5

"LP" and "CP" denote "linear polarization" and "circular polarization," respectively.

III. PERFORMANCE

To validate the concept of the HMSIW-fed aperture-coupled DRAs, both a linearly polarized antenna and a circularly polarized antenna have been designed following the procedures above and optimized with the aid of the simulation tool HFSS. Both antennas are designed to operate at around 60 GHz and their dimensions are listed in Table I. In both cases, the substrate made of Rogers 5880 has a thickness $t = 0.127$ mm, a permittivity $\varepsilon_r = 2.2 \pm 0.02$, and a loss tangent of 0.001. The dielectric cylinders used for both antennas are made of Rogers TMM10i with a permittivity $\varepsilon_r = 10.0 \pm 0.2$ and a loss tangent of 0.002. The dielectric cylinders are glued over the slot on the HMSIW conducting back plane using Araldite resin with a permittivity $\varepsilon_r = 3.6$ and an estimated loss tangent of 0.06 at 2.45 GHz [28], [29]. The glue layer labeled as "h_{g}" in Fig. 1(c) is estimated 15 ± 5 μm thick. Simulated performance of the two designs has been compared to the experimental results of two corresponding fabricated prototypes. Before conducting a quantitative discussion on the comparison, it is worth pointing out that all electrical characteristics of the two Rogers dielectric materials above, i.e., Rogers 5880 and Rogers TMM10i, are specified at 10 GHz by their manufacturer [30]. However, considering the reported stability of those materials properties [31], [32], it has been empirically assumed in our design that the variation of the material properties with frequency is still within tolerance even up to 60 GHz. The results in the following section validate this assumption through a good agreement between simulations and measurements.

In order to investigate the influence of glue layer on the antenna performance, the linearly polarized HMSIW-fed DRA has been numerically analyzed with glue layers of different thicknesses $h_g = 10$, 15, and 20 μm, respectively. From the resulting reflection coefficient curves plotted in Fig. 4, it can be seen that even a slight increase in the glue layer thickness can significantly influence the impedance matching over the whole band. Therefore, it is crucial to take the glue layer effects into account while designing DRAs operating in the millimeter-wave band. The simulated input impedance obtained from the use of a 15 μm thick glue layer is also depicted in the inset of Fig. 4. A lower resonance due to the slot occurs at around 46 GHz, whereas the higher offset resonance caused by the dielectric resonator cylinder is observed at around 60 GHz.

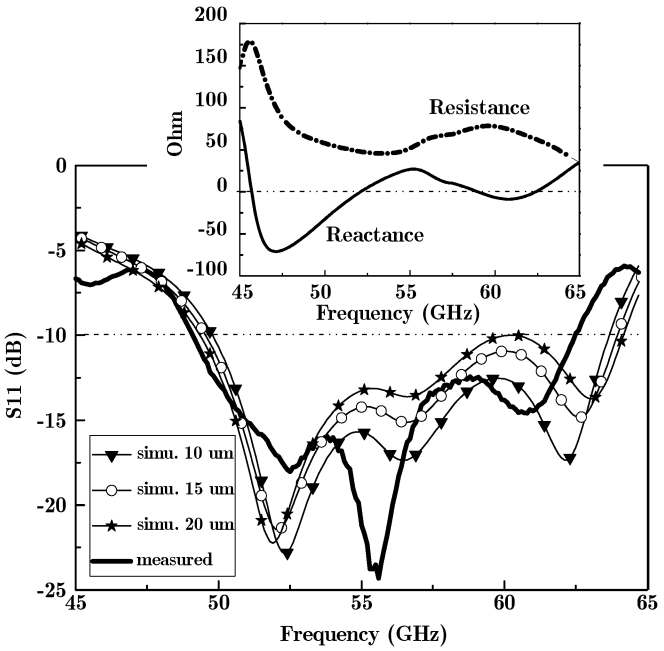

Fig. 4. Simulated and measured reflection coefficients of the linearly polarized HMSIW-fed DRA. The simulation results are obtained with the use of different glue layer thicknesses, i.e., $h_g = 10$, 15, and 20 μm. The inset depicts the simulated input impedance obtained in the case of 15 μm thick glue layer.

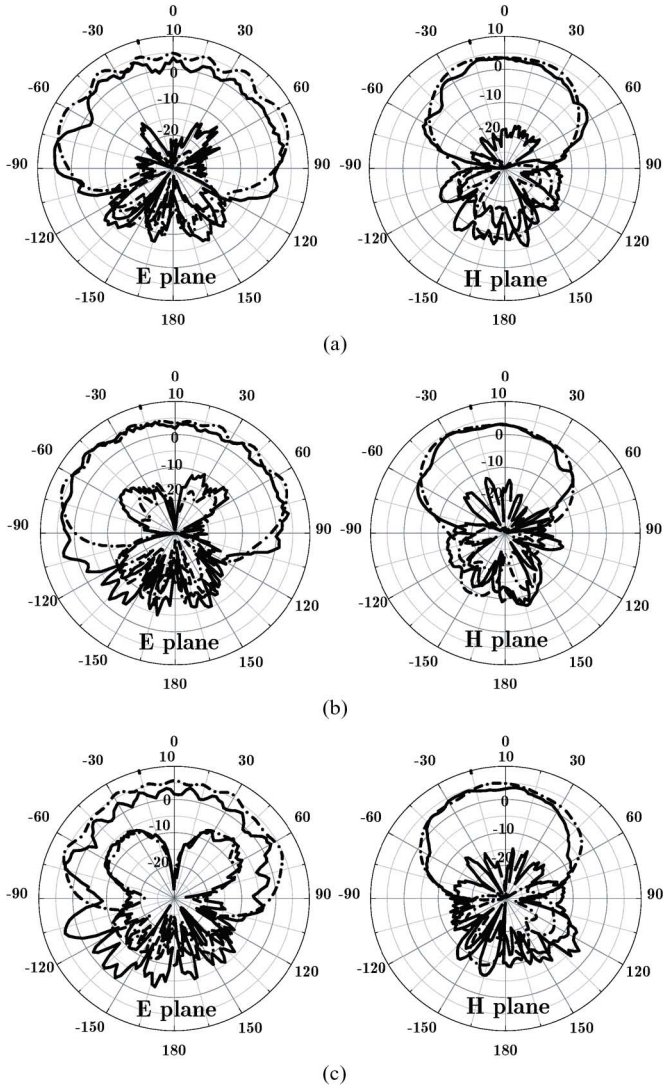

Fig. 5. Co- and cross-polarized radiation patterns of the linearly polarized HMSIW-fed DRA at (a) 50 GHz, (b) 55 GHz, and (c) 63 GHz. The measurement results are presented in solid line, while the simulation results in dash line.

The measured reflection coefficient is also shown in Fig. 4, presenting a bandwidth of 24.0% for $S_{11} < -10$ dB. By contrast, a bandwidth of 25.5% is obtained in the simulation using the 15 μm thick glue layer. These results confirm that offset resonances of the slot and the dielectric resonator can be combined to achieve broadband operation.

The radiation patterns obtained at three frequency points, i.e., 50 GHz, 55 GHz, and 63 GHz, are illustrated in Fig. 5. All patterns are broadside and correspond to the pattern of a horizontal magnetic dipole on the ground plane. This is expected for both the $HEM_{11\delta}$ DR mode and for the slot resonance. In both simulations and measurements, ripples are observed in the E-plane pattern over the whole operation band, which can mainly be explained by diffraction at the edges of the finite ground plane. The level of ripples measured at the antenna broadside is about 2.2 dB at 50 GHz, 0.9 dB at 55 GHz, and 2.4 dB at 63 GHz.

As for radiation patterns in the H-plane, the measured pattern has a 3 dB beamwidth of 76° at 50 GHz, of 60° at 55 GHz, and of 74° at 63 GHz. All angles above are estimated in an error of 2°. Due to the finite dimension of the ground plane, a relatively large back radiation occurs in both E and H plane patterns. Radiation leakage from the HMSIW open side causes the asymmetry in the H plane pattern.

Similarly as in the analysis of reflection coefficient, the near broadside maximum gain of the linearly polarized antenna is also investigated with the aid of the simulation tool HFSS for three different thicknesses of the glue layer, i.e., $h_g = 10$ μm, 15 μm, and 20 μm. The simulation results are plotted as a function of frequency in Fig. 6, showing that a change of 5 μm in the glue layer thickness with an estimated loss tangent of 0.06 can lead to a shift of 0.10 ± 0.07 dB in the maximum gain over the whole operation band. In addition, the measured gain is also illustrated in Fig. 6, exhibiting a level of above 5.5 dB in the frequency range of 49.5 to 62.5 GHz. Variations observed in the measurement data can mainly be explained by large ripples in the radiation patterns (as shown in Fig. 5) and uncertainties in the measurements. It is noted that the measured gain shown in Fig. 6 is calibrated by removing the losses in the feeding structure composed of a 90 degree bend and an MMPX connector, which are experimentally estimated at about 0.5 ± 0.1 dB from 50 GHz to 56 GHz, about 0.6 ± 0.1 dB from 56 GHz to 58 GHz, and about 0.9 ± 0.1 dB above 60 GHz. The discrepancy between the measured and simulated results is mainly attributed to some experimental losses unaccounted for in the simulations.

The radiation efficiency of the linearly polarized HMSIW-fed DRA has been measured using the directivity/gain method (D/G method) [17], [33], [34]. For this measurement, the gain is directly measured with a reference standard gain horn in an anechoic chamber. To determine the directivity with reasonable measurement accuracy [17], both the co- and cross-polarized 3D radiation patterns of the DRA are first sampled with an azimuth

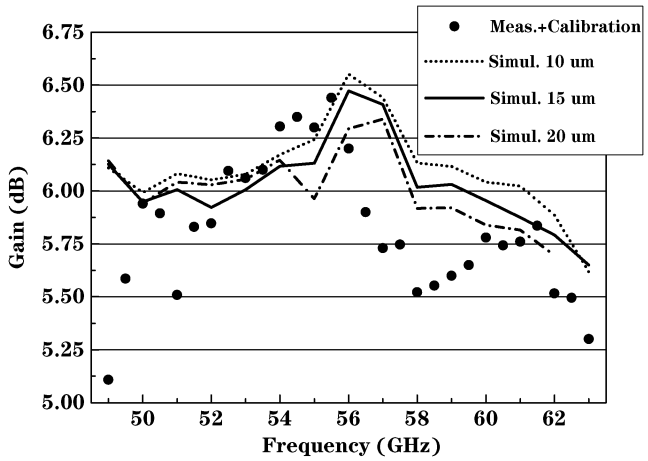

Fig. 6. Gain vs. frequency for the linearly polarized HMSIW-fed DRA. The simulated gain is obtained with the use of different glue layer thicknesses, i.e., $h_g = 10$, 15, and 20 μm. The measured data are calibrated with the experimentally estimated losses of a 90 degree bend and an MMPX connector, which are used for feeding the antenna.

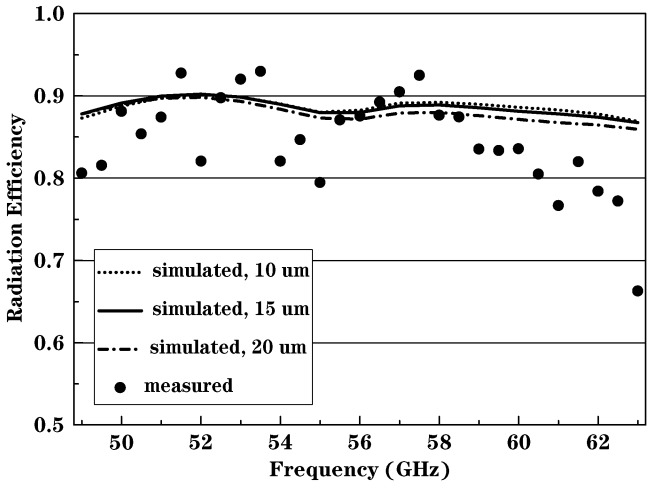

Fig. 7. Radiation efficiency of the linearly polarized HMSIW-fed DRA. The simulated results are obtained with the use of different glue layer thicknesses, i.e., $h_g = 10$, 15, and 20 μm. The losses due to the 90 bend, MMPX connector, and microstrip line together with the taper transition have been excluded from the measured radiation efficiency.

interval of 10° and an elevation interval of 2°. Subsequently, the directivity is calculated through a numerical integration over the sampled 3D patterns [33]. Lastly, the radiation efficiency of interest can be computed according to its definition, i.e., division of the gain by the directivity. On the side of the simulation, the radiation efficiency (labeled as "simulated" in Fig. 7) can also be accurately determined using the same procedure, in which however, the gain and 3D radiation patterns are provided by simulations.

Fig. 7 depicts the radiation efficiency obtained from simulations and measurements. Firstly, a comparison of the simulated radiation efficiency obtained for different glue layer thicknesses, i.e., $h_g = 10$ μm, 15 μm, and 20 μm, shows that the impact of a small change (≤ 10 μm) in the glue layer thickness on the radiation efficiency is not significant for the presently used glue. This finding is consistent with the fact that the gain is only slightly affected by the specified variations of the glue

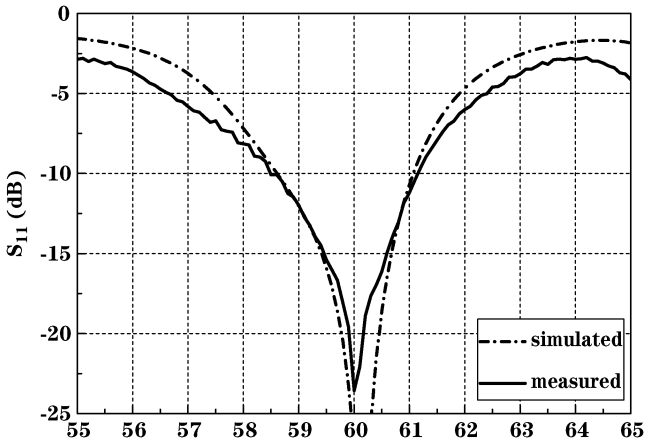

Fig. 8. Reflection coefficient of the circularly polarized HMSIW-fed DRA.

layer, as discussed for Fig. 6. Secondly, as the present investigation aims at characterizing the combination of the dielectric resonator and its feeding HMSIW, the losses due to the 90 degree bend, the MMPX connector, and the microstrip line together with the taper transition have been excluded from the measured radiation efficiency. The losses in the bend and connector are as given previously in the discussion of Fig. 6, while those due to the microstrip line and the taper transition are experimentally estimated about 0.3 ± 0.1 dB over the whole operation band. Therefore, the radiation efficiency presented in Fig. 7 only includes the dielectric losses of the cylindrical resonator, as well as the dielectric and conductor losses of the feeding HMSIW. From Fig. 7, it can be seen that the measured radiation efficiency exhibits a maximum of 92% around 57 GHz and generally stays above 80% over the whole operation band, indicating that the HMSIW can be an efficient feed for DRAs operating around 60 GHz. Variations in the measured gain as shown in Fig. 6 contributes directly to significant spread in the measured radiation efficiency. The discrepancy between the measurement and simulation results mainly arises from some unaccounted losses and from uncertainties in the measurements which is considered an intrinsic drawback of the D/G method [17], [34].

In summary, the measured performance of the linearly polarized HMSIW-fed DRA demonstrates attractive characteristics in terms of bandwidth and radiation efficiency.

The following discussion will now focus on the performance of the circularly polarized HMSIW-fed DRA. First, the measured reflection coefficient is presented in Fig. 8, exhibiting a bandwidth of 4.5% or 2.7 GHz for $S_{11} < -10$ dB. Then, Fig. 9 depicts the axial ratio (AR) measured at the antenna boresight, demonstrating a 3-dB AR bandwidth of 4.0%, i.e., from 58.6 to 61.0 GHz, with a minimum of about 0.8 dB around 59.5 GHz. A comparison between the frequency responses in Fig. 8 and Fig. 9 reveals that the antenna operates with AR < 3 dB at the broadside over most of the operation band.

Fig. 10 plots the measured major and minor axes of the polarization ellipse as a function of the elevation angle in two orthogonal planes, i.e., the yz- and xy-plane as defined in Fig. 1(a) at 59.4 GHz. The results show that the beamwidth for AR $<$ 3 dB is 81° in the yz-plane (from $-19°$ to 62°) and 99° in the xy-plane (between $-44°$ and 55°).

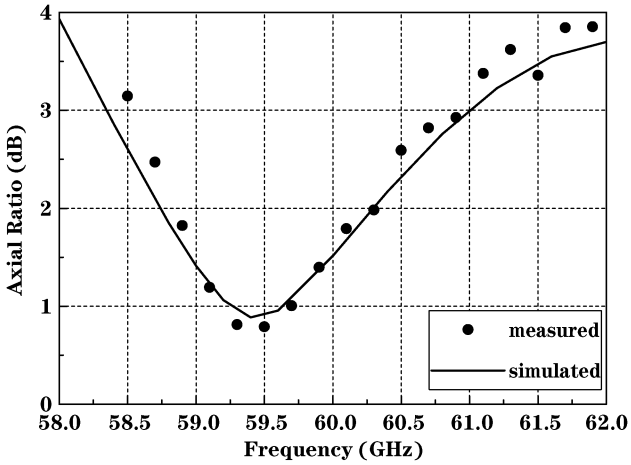

Fig. 9. Axial ratio at the broadside of the circularly polarized HMSIW-fed DRA.

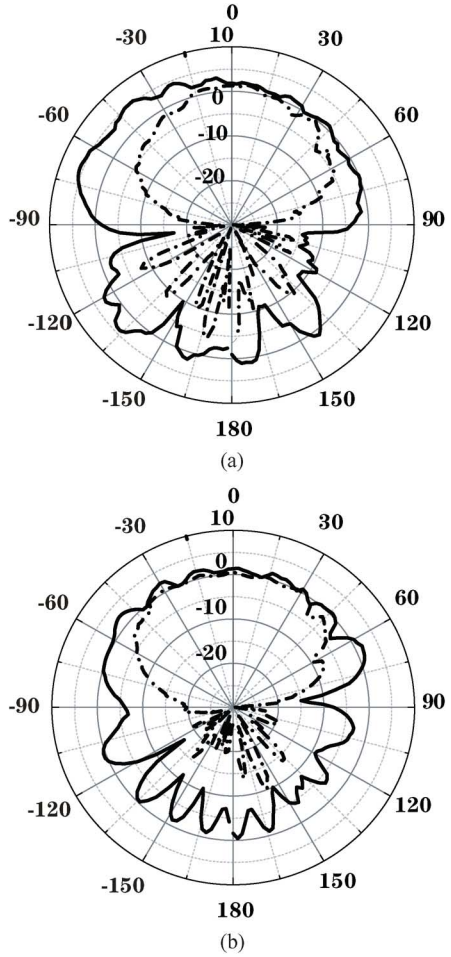

Fig. 10. Measured major and minor axes of the polarization ellipse vs. elevation angle in the (a) yz-plane and (b) xy-plane for the circularly polarized HMSIW-fed DRA at 59.4 GHz. The coordinates are as shown in Fig. 1(a). The major axis is plotted in solid line, while the minor axis in dash line.

Up to this point, the simulated and measured performance has been demonstrated for both the linearly and circularly polarized HMSIW-DRA. With the attractive features of those single antennas, it appears desirable to assemble them in a linear or planar array. The combination of a low-loss transmission line with a highly efficient antenna strongly suggests the possibility achieving significantly higher radiation efficiency than with conventional microstrip-fed patch antennas arrays. The challenges towards realization of arrays can be described in terms of design and fabrication.

On the side of the design, a relatively straightforward realization of a linear array would make use of a resonant series array of $1 \times N$ DRAs fed by a common end-shorted HMSIW. This array can be analyzed and designed using an approach similar to that for the resonant slot array fed by an HMSIW [21] or by a boxed stripline [35]. For application where frequency scanning is not desired, a corporate feed based on multi-way T-junctions [22] would need to be realized, while accommodating the larger transverse directions of the HMSIW compared to the microstrip line. This might increase the overall complexity, especially for a planar array. However, as the HMSIW can be considered as a nearly closed structure on the side of its vias, it can be intuitively expected that the mutual coupling between parallel HMSIWs will be lower than that of parallel microstrip lines in a feeding network, allowing to place them in close proximity. A detailed investigation of the mutual coupling between HMSIWs will be the subject of a future communication.

On the side of the fabrication, the realization of a large number of metalized via holes in a circuit will certainly increase the complexity of the physical realization. However, in the context of the application of 3D multi-layer techniques such as Low-Temperature Co-fired Ceramic (LTCC) technology, the realization of such vias appears realistically feasible. Another practical alternative for standard planar circuit technology is to replace the row of vias in each HMSIW with a narrow longitudinal slot cut through the substrate. The inner surface of the slot needs to be metalized to realize the electric wall and to prevent the wave leakage.

IV. Conclusion

This paper has proposed an HMSIW-fed dielectric resonator antenna. The combination of an efficient feeding transmission line with an efficient radiator allows achieving a radiation efficiency above 80% around 60 GHz, with a maximum of 92%. The attractive performance of two HMSIW-fed DRA prototypes at 60 GHz, respectively for linear polarization and for circular polarization, has been substantiated in terms of bandwidth and radiation efficiency through simulations and experiments. The results demonstrate the feasibility of the HMSIW as an *efficient* feed for DRAs operating in the millimeter wave frequency band. The individual HMSIW-fed DRA can further be applied as an element for constructing HMSIW-fed series arrays or planar arrays of DRAs.

Acknowledgment

The authors thank H. Benedickter and G. Almpanis (ETH Zurich) for their helpful discussion and kind assistance in the measurement. The authors are also grateful to M. Lanz and C. Maccio (ETH Zurich) for their excellent manufacture of the devices.

REFERENCES

[1] S. A. Long, M. W. McAllister, and L. C. Shen, "The resonant cylindrical dielectric cavity antenna," *IEEE Trans. Antennas Propag.*, vol. 31, no. 3, pp. 406–412, May 1983.

[2] K. W. Leung, K. M. Luk, and K. Y. A. Lai, "Theory and experiment of a coaxial probe fed dielectric resonator antenna," *IEEE Trans. Antennas Propag.*, vol. 41, no. 10, pp. 1390–1398, Oct. 1993.

[3] G. P. Junker, A. A. Kishk, and A. W. Glisson, "Input impedance of dielectric resonator antennas excited by a coaxial probe," *IEEE Trans. Antennas Propag.*, vol. 42, no. 7, pp. 960–966, Jul. 1994.

[4] R. A. Karnenburg and S. A. Long, "Microstrip transmission line excitation of dielectric resonator antennas," *Electron. Lett.*, vol. 24, no. 18, pp. 1156–1157, Sep. 1988.

[5] R. Kranenberg, S. A. Long, and J. T. Williams, "Coplanar waveguide excitation of dielectric resonator antennas," *IEEE Trans. Antennas Propag.*, vol. 39, no. 1, pp. 119–122, Jan. 1991.

[6] M. T. Birand and R. V. Gelsthorpe, "Experimental millimetric array using dielectric radiators fed by means of dielectric waveguide," *Electron. Lett.*, vol. 13, no. 18, pp. 633–635, Sep. 1981.

[7] K. W. Leung and K. K. So, "Rectangular waveguide excitation of dielectric resonator antenna," *IEEE Trans. Antennas Propag.*, vol. 51, pp. 2477–2481, Sep. 2003.

[8] J. T. H. ST. Martin, Y. M. M. Antar, A. A. Kishk, A. Ittipiboon, and M. Cuhaci, "Dielectric resonator antenna using aperture coupling," *Electron. Lett.*, vol. 26, pp. 2015–2016, Sep. 1990.

[9] K. W. Leung, K. M. Luk, K. Y. A. Lai, and D. Lin, "Theory and experiment of an aperture coupled hemispherical dielectric resonator antenna," *IEEE Trans. Antennas Propag.*, vol. 43, no. 9, pp. 1192–1198, Nov. 1995.

[10] R. N. Simons and R. Q. Lee, "Effect of parasitic dielectric resonators on CPW/aperture coupled dielectric resonator antennas," *IEE Micorw. Antennas Propag.*, vol. 140, no. 5, pp. 336–338, Oct. 1993.

[11] Z. C. Hao, W. Hong, A. D. Chen, J. X. Chen, and K. Wu, "SIW fed dielectric resonator antennas," in *Proc. Int. Symp. Microw. Theory Tech.*, San Francisco, Jun. 2006, pp. 202–205.

[12] C. Y. Huang, J. Y. Wu, and K. L. Wong, "Cross slot coupled microstrip antenna and dielectric resonator antenna for circular polarization," *IEEE Trans. Antennas Propag.*, vol. 47, no. 4, pp. 605–609, Apr. 1999.

[13] K. W. Leung, W. C. Wong, and H. K. Ng, "Circularly polarized slot coupled dielectric resonator antenna with a parasitic patch," *IEEE Antennas Wireless Propag. Lett.*, vol. 1, pp. 57–59, Jul. 2002.

[14] G. Almpanis, C. Fumeaux, and R. Vahldieck, "Offset cross slot coupled dielectric resonator antenna for circular polarization," *IEEE Microw. Wireless Compon. Lett.*, vol. 16, no. 8, pp. 461–463, Aug. 2006.

[15] M. B. Oliver, Y. M. M. Antar, R. K. Mongia, and A. Ittipiboon, "Circularly polarized rectangular dielectric resonator antenna," *Electron. Lett.*, vol. 31, no. 6, pp. 418–419, Mar. 1995.

[16] A. Buerkle, K. Sarabandi, and H. Mosallaei, "Compact slot and dielectric resonator antenna with dual resonance, broadband characteristics," *IEEE Trans. Antennas Propag.*, vol. 53, no. 3, pp. 1020–1027, Mar. 2005.

[17] Q. H. Lai, C. Fumeaux, W. Hong, and R. Vahldieck, "Comparison of the radiation efficiency for the dielectric resonator antenna and the microstrip antenna at Ka band," *IEEE Trans. Antennas Propag.*, vol. 56, no. 11, pp. 3589–3592, Nov. 2008.

[18] W. Hong, B. Liu, Y. Wang, and Q. Lai *et al.*, "Half mode substrate integrated waveguide: A new guided wave structure for microwave and millimeter wave application," in *Proc. Joint 31st Int. Conf Infra. Millimeter Waves/14th Int. Conf. Terahertz Electron.*, Shanghai, Sep. 2006, pp. 18–22.

[19] Y. Wang, W. Hong, Y. Dong, and B. Liu *et al.*, "Half mode substrate integrated waveguide (HMSIW) bandpass filter," *IEEE Microw. Wireless Compon. Lett.*, vol. 17, no. 4, pp. 256–267, Apr. 2007.

[20] Y. Cheng, W. Hong, and K. Wu, "Half mode substrate integrated waveguide (HMSIW) directional filter," *IEEE Microw. Wireless Compon. Lett.*, vol. 17, no. 7, pp. 504–506, Jul. 2007.

[21] Q. H. Lai, W. Hong, Z. Q. Kuai, Y. S. Zhang, and K. Wu, "Half mode substrate integrated waveguide transverse slot array antennas," *IEEE Trans. Antennas Propag.*, vol. 57, no. 4, pp. 1064–1072, Apr. 2009.

[22] B. Liu, W. Hong, L. Tian, H. B. Zhu, W. Jiang, and K. Wu, "Half mode substrate integrated waveguide (HMSIW) multi-way power divider," in *Proc. Asia Pacific Microw. Conf.*, Suzhou, China, Dec. 12–15, 2006, pp. 917–920.

[23] Q. H. Lai, C. Fumeaux, W. Hong, and R. Vahldieck, "Characterization of the propagation properties of the half-mode substrate integrated waveguide," *IEEE Trans. Microw. Theory Tech.*, vol. 57, no. 8, pp. 1996–2004, Aug. 2009.

[24] F. Xu and K. Wu, "Guided-wave and leakage characteristics of substrate integrated waveguide," *IEEE Trans. Microw. Theory Tech.*, vol. 53, no. 1, pp. 66–72, Jan. 2005.

[25] R. K. Mongia and P. Bhartia, "Dielectric resonator antennas—A review and general design relations for resonant frequency and bandwidth," *Int. J. Microw. Millim.-Wave Comput.-Aided Eng.*, vol. 4, no. 3, pp. 230–247, Mar. 1994.

[26] K. M. Luk and K. W. Leung, *Dielectric Resonator Antennas*. Hertfordshire, England: Research Studies Press, 2002, pp. 179–183.

[27] A. J. Simmons, "Circularly polarized slot radiators," *IEEE Trans. Antennas Propag.*, vol. 5, no. 1, pp. 31–36, Jan. 1957.

[28] Huntsman Advanced Materials American Inc., 2004, Product Data Araldite AW 106 Resin [Online]. Available: http://adhesive.leaderseal.com/download/TDS-A106-953(US).pdf

[29] M. J. Akhtar, L. Feher, and M. Thumm, "Measurement of dielectric constant and loss tangent of epoxy resins using a waveguide approach," in *Proc. IEEE Antenna Propag. Symp.*, Albuquerque, NM, Jul. 9–14, 2006, pp. 3179–3182.

[30] Rogers Corporation, 1991–2002, High Frequency Circuit Materials Product Selector Guide [Online]. Available: http://www.leiton.de/formulare/Rogers.pdf

[31] G. J. Simonis, J. P. Satter, T. L. Worchesky, and R. P. Leavitt, "Characterization of near millimeter wave materials by means of non-dispersive Fourier transform spectroscopy," *Int. J. Infrared Millim. Wave*, vol. 5, no. 1, pp. 57–72, May 1984.

[32] V. N. Egorov, V. L. Masalov, Y. A. Nefyodov, A. F. Shevchun, and M. R. Trunin, "Measuring microwave properties of laminated dielectric substrates," *Rev. Sci. Instrum.*, vol. 75, no. 11, pp. 4423–4433, Nov. 2004.

[33] C. A. Balanis, *Antenna Theory*. Hoboken, NJ: Wiley, 2005, pp. 1028–1036.

[34] D. M. Pozar and B. Kaufman, "Comparison of three methods for the measurement of printed antenna efficiency," *IEEE Trans. Antennas Propag.*, vol. 36, no. 1, pp. 136–139, Jan. 1988.

[35] R. Shavit and R. S. Elliott, "Design of transverse slot arrays fed by a boxed stripline," *IEEE Trans. Antennas Propag.*, vol. 31, no. 4, pp. 545–552, Jul. 1983.

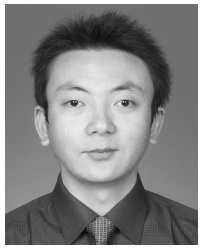

Qinghua Lai (S'09) received the B.S. degree in radio engineering from University of Electronic Science and Technology, Chengdu, China, in 2004. He is currently working toward the M.Phi. and Ph.D. degrees in radio engineering at Southeast University, Nanjing, China.

From July 2007 to June 2008, he was Visiting Student with the Swiss Federal Institute of Technology (ETH), Zurich, Switzerland, where he was engaged in the research on the radiation efficiency of dielectric resonator antennas and on the propagation properties of half-mode substrate integrated waveguides. From September 2008 to September 2009, he was a Academic Guest with ETH, where he was involved in the development of high-performance filter for the base station. His current research interests focus on array antennas and filters.

Christophe Fumeaux (M'03–SM'09) received the Diploma and Ph.D. degrees in physics from the ETH Zurich, Switzerland, in 1992 and 1997, respectively.

From 1998 to 2000, he was a Postdoctoral Researcher with the School of Optics, University of Central Florida, Orlando. In 2000, he joined the Swiss Federal Office of Metrology, Bern, Switzerland, as a Scientific Staff Member. From 2001 to 2008, he was a Research Associate and Group Leader with the Laboratory for Electromagnetic Fields and Microwave Electronics (IFH), ETH, Zurich, Switzerland. During the Fall of 2005, he was a Visiting Scientist with the Laboratory of Sciences and Materials for Electronics, and of Automatic (LASMEA), University Blaise Pascal, Clermont-Ferrand, France. In 2008, he joined the School of Electrical and Electronic Engineering, the University of Adelaide, Australia, as an Associate Professor. His current main research interest concerns computational electromagnetics, microwave circuits and antenna engineering.

Dr. Fumeaux was the recipient of the ETH Silver Medal of Excellence for his doctoral dissertation. From 2006 to 2008, he was the Chairman of the IEEE Swiss Joint Chapter on Microwave Theory and Techniques, Antennas and Propagation, and EMC. He was the corecipient of the outstanding paper award of the Applied Computational Electromagnetics Society (ACES) in 2004.

Wei Hong (M'92–SM'07) received the B.S. degree from the University of Information Engineering, Zhengzhou, China, in 1982, and the M.S. and Ph.D. degrees from Southeast University, Nanjing, China, in 1985 and 1988, respectively, all in radio engineering.

Since 1988, he has been with the State Key Laboratory of Millimeter Waves, Southeast University, where he is currently a Professor with the School of Information Science and Engineering. In 1993 and 1995–1998, he was a short-term Visiting Scholar with the University of California at Berkeley and the University of California at Santa Cruz. He has been engaged in numerical methods for electromagnetic problems, millimeter-wave theory and technology, antennas, electromagnetic scattering, RF technology for mobile communications, etc. He has authored or coauthored over 200 technical publications. He authored *Principle and Application of the Method of Lines* (in Chinese) (Southeast Univ. Press, 1993) and *Domain Decomposition Methods for Electromagnetic Problems* (in Chinese) (Sci. Press, 2005). He has served as a reviewer for *IET Microwave Antennas, and Propagation and Electronics Letters*.

Dr. Hong is a Senior Member of the Chinese Institute of Electronics (CIE). He is vice president of the Microwave Society and Antenna Society, CIE. He has served as a reviewer for the IEEE TRANSACTIONS ONMICROWAVE THEORY AND TECHNIQUES and the IEEE TRANSACTIONS ON ANTENNAS AND PROPAGATION. He is an associate editor for the IEEE TRANSACTIONS ON MICROWAVE THEORY AND TECHNIQUE. He was a two-time recipient of the 1992 and 1994 First-Class Science and Technology Progress Prizes presented by the Ministry of Education of China and the 1991 Fourth-Class National Natural Science Prize. He was also the recipient of the Foundations for China Distinguished Young Investigators and for the "Innovation Group" presented by the National Natural Science Foundation of China (NSFC).

Rüdiger Vahldieck (M'85–SM'86–F'99) received the Dipl.-Ing. and the Dr.-Ing. degrees in electrical engineering from the University of Bremen, Germany, in 1980 and 1983, respectively.

He was a Postdoctoral Fellow with the University of Ottawa, Ottawa, ON, Canada, until 1986. In 1986, he joined the Department of Electrical and Computer Engineering, University of Victoria, BC, Canada, where he became a Full Professor in 1991. During Fall and Spring of 1992 to 1993 he was a Visiting Scientist at the "Ferdinand-Braun-Insitute fór Hochfrequenztechnik", Berlin, Germany. In 1997, he was appointed Professor for electromagnetic field theory at the Swiss Federal Institute of Technology, Zurich, and became head of the Laboratory for Electromagnetic Fields and Microwave Electronics (IFH) in 2003. In 2005, he became President of the Research Foundation for Mobile Communications and was elected Head of the Department of Information Technology and Electrical Engineering (D-ITET), ETH Zurich. Since 1981 he has published more than 300 technical papers in books, journals and conferences. His research interests include computational electromagnetics in the general area of EMC and in particular for computer-aided design of microwave, millimeter wave and optoelectronic integrated circuits.

Dr. Vahldieck received the Outstanding Publication Award of the Institution of Electronic and Radio Engineers in 1983, the K.J. Mitra Award of the IETE (in 1996) for the best research paper in 1995, and the ACES Outstanding Paper Award in 2004. He is the Past-President of the IEEE 2000 International Zurich Seminar on Broadband Communications (IZS'2000) and since 2003 President and General Chairman of the international Zurich Symposium on Electromagnetic Compatibility (EMC Zurich). He is a member of the editorial board of the IEEE TRANSACTIONS ON MICROWAVE THEORY AND TECHNIQUES. From 2000 until 2003 he served as Associate Editor for the IEEE MICROWAVE AND WIRELESS COMPONENTS LETTERS and from July 2003 until the end of 2005 as the Editor-in Chief. Since 1992, he has been on the Technical Program Committee of the IEEE International symposium, the MTT-S Technical Committee on Microwave Field Theory, and in 1999 on the TPC of the European Microwave Conference. From 1998 until 2003 he was the Chapter Chairman of the IEEE Swiss Joint Chapter on MTT, AP, and EMC.